Received 19 December 2023; revised 19 January 2024; accepted 27 January 2024. Date of publication 1 February 2024; date of current version 22 November 2024.

Digital Object Identifier 10.1109/OJAP.2024.3361381

Compact High Gain Wideband Circularly Polarized Non-Uniform Metasurface Antenna Through Improved Mode Coupling

KOMAL IQBAL, QASIM UMAR KHAN (Member, IEEE), AND ZUBAIR AHMED

Department of Electrical Engineering, College of Electrical and Mechanical Engineering, National University of Sciences and Technology, Islamabad 44000, Pakistan

CORRESPONDING AUTHOR: Q. U. KHAN (e-mail: qasimumarkhan@yahoo.com)

ABSTRACT A wideband, high gain circularly polarized (CP) metasurface (MTS) based slot antenna is presented. The designed nonuniform slots provide wider bandgap regions and extra degree of freedom in tuning to obtain wider impedance bandwidth through improved mode coupling for fixed optimum feed location along with improved 3-dB axial ratio bandwidth and gain. The extra radiation edges provided by nonuniform slots within the unit cell help in improving mode coupling thus resulting in increased performance of the designed antenna. Improved mode coupling in case of the proposed antenna is explained and verified using characteristic mode analysis (CMA). The proposed antenna with a small size of 0.8 x 0.8 x 0.079 λ_0^3 (λ_0 at 6 GHz) is designed. Based on the proposed analysis, an antenna having wide impedance bandwidth of 48.74% (5.74-9.44 GHz), and a 3-dB axial ratio (AR) bandwidth of 19.92% (6.19-7.56 GHz) with a peak gain of 9.35 dBi is designed. In addition, a 2 x 2 array of proposed MTS is designed and fabricated. The MTS array has a peak gain of 14.45dBi with a 3-dB AR bandwidth of 61.75% and impedance bandwidth of 71.71%. The proposed antennas find good use in WiMAX, C-band, and radars applications.

INDEX TERMS Non-uniform metasuraface, circular polarization, high gain, wideband antenna.

I. INTRODUCTION

HIGH gain, wideband, and circular polarized antennas are one of the key requirements in communication systems. To achieve these traits, microstrip patch antennas are one of the choices [1], [2], [3]. However, patch antennas have narrow impedance bandwidth (IBW) and 3-dB axial ratio bandwidth (ARBW) for circular polarization along with low gain. Recently, use of metasurfaces (MTS) is gaining importance for enhancing antenna performance. The effective approach of enhancing antenna's performance matrices is the placement of metasurface either above or below the radiating element. This approach got significant attention due to the unique concept of generating extra resonances by the surface waves' excitation of radiating patch, leading to the overall increase in the IBW and 3-dB ARBW [4], [5], [6]. Metasurface comprised of an array of unit cells used in [4], [5], [6] block the flow to surface currents along the sheet. Such metasurfaces help in exciting surface waves by means of unit cells to generate extra resonances that eventually increase the bandwidth. Utilizing this notion, the significant increase in the IBW (42.1%, 45.6%, 43.2%) and 3-dB ARBW (30%, 23.4%, 22%) of designed antennas were reported in [4], [5], [6], respectively. Although, such MTS-based patch antennas effectively widen the bandwidths but their low gain ranging from 6.16-7.6 dBi make the designs not so preferable for certain high gain applications. To overcome this issue, MTS radiated through the coupling slots effectively resulted in high gain along with wideband bandwidth, and 3-dB ARBW [7], [8], [9], [10], [11], [12]. A common type of antenna improving the performance matrices is the Fabry-Perot resonator antenna (FPRA) [8], [9]. Undoubtedly, FPRAs are very popular in achieving high gain with wideband properties but their mechanical fragility due to the presence of air gap and relatively high profile limit their application. Therefore, the alternate approach of realizing low-profile antennas without air gap has been adopted frequently in [10], [11], [12].

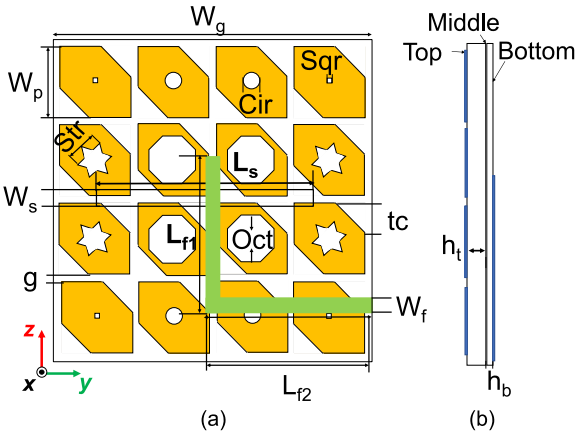

FIGURE 1. Geometry of Proposed Metasurface Antenna. (a) Front-view, (b) Side-view. The optimized design parameters are: $W_g = 40$mm, $W_p = 9$mm, g = 1mm, $L_{f1} = L_{f2} = 20$mm, $W_s = 2.8$mm, $L_s = 28$mm, $W_f = 1.81$mm, $h_t = 3.18$mm, $h_b = 0.787$ mm, tc = 2.83mm, Cir = 1.7mm, Sqr = 0.5mm, Oct = 5.93mm, and Str = 3.9mm.

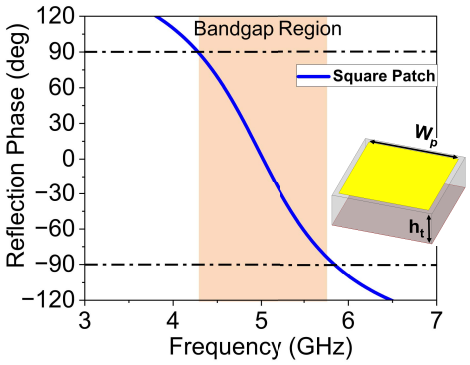

FIGURE 2. Structure and reflection phase of square unit cell. $W_p = 9$ mm, $h_t = 3.18$ mm $\varepsilon_r = 2.2$, tan$\delta = 0.0009$.

In addition, characteristic mode analysis (CMA) has been effectively used for antenna design and subsequently its analysis. For example, the potential application of CMA for realizing wideband antennas was reported in [13], [14], [15] where multiple resonances were simultaneously excited, leading to the wideband antennas. However, these proposed antennas were either linearly polarized [13], [14] or circularly polarized with narrower impedance bandwidth, i.e., 25% [15]. Apart from single element MTS, the bandwidth and gain were improved by the use of array configurations in [19], [20], [21], [22] at the expense of large size and low 3-dB axial ratio bandwidth. To summarize, these different design approaches resulted in improvement of either antenna impedance and 3-dB axial ratio bandwidths [4], [5], [6], [11], [12] but with low gain, or when tried to improve gain along with IBW and 3-dB ARBW resulted in high profile and/or large size [7], [8], [9], [10]. These performance traits are not simultaneously achieved in a single design. In this article, a novel non-uniformly slotted MTS-based low-profile antenna is proposed to improve the antenna's bandwidth, gain, and axial ratio, while preserving antenna's compactness. Such an MTS is excited by an L-shaped microstrip feedline through a slot in the ground plane. The article is arranged as follows: Section II gives the overview for the proposed antenna geometry. In Section III, a detailed analysis of the working mechanism of the designed antenna is presented along with the explanation of circular polarization. Section IV discusses simulated and measured results of a single element metasurface antenna. Section V presents the array configuration of the proposed antenna to further improve gain and 3-dB axial ratio bandwidth, trailed by the conclusion in Section VI.

II. DESIGN OF PROPOSED ANTENNA ELEMENT

The geometry of the proposed MTS antenna designed for C-band is illustrated in Fig. 1. The antenna comprises of two Rogers RO5880 substrates ($\varepsilon_r = 2.2$, tan$\delta = 0.0009$) with thicknesses of $h_t = 3.18$ mm and $h_b = 0.787$ mm. The upper substrate of thickness h_t incorporates the top (MTS) layer, while the lower substrate of thickness h_b is provided for the middle ground plane and bottom microstrip feedline layers. The proposed MTS consists of 4x4 square metal patches of the size W_p and the patch-to-patch gap of 'g' placed on the top surface. Slots of different shapes and sizes are etched from these patches and the corners of each patch are truncated. A square ground plane of size W_g is sandwiched between the top and bottom substrates. The ground plane contains a slot of width W_s and length L_s located in the center of the plane. On the bottom of the second substrate, L-shaped microstrip feedline is placed.

III. DESIGN GUIDELINES AND WORKING PRINCIPLE OF THE PROPOSED ANTENNA

A. DESIGN GUIDELINES

Metasurface is the engineered structure composed of the surface distribution of electrically small resonators, commonly known as unit cells [16]. The size 's' of each unit cell lies within the range of effective homogeneity limit (EHL), i.e., $\lambda_0/20 \leq s \leq \lambda_0/4$ [16], where λ_0 is the wavelength at 5 GHz. The antenna design starts with a simple square shaped unit cell designed at 5GHz with size Wp = 9mm for EHL= $\lambda_0/7$. This unit cell is analyzed using floquet-port HFSS model that provides the in-phase reflection property. The response shown in Fig. 2 reveals that the bandgap region over which the reflection phase lies between $+90°$ to $-90°$ supports in-phase reflections due to high impedance. In this range of frequencies (or radiation bandwidth, i.e., 4.3 GHz to 5.7 GHz) the radiation efficiency is high. We suggest the readers to follow [16] for the detailed insight about how radiation efficiency is related to the radiation bandwidth of a unit cell.

To instil nearby resonances that will widen the bandgap region and improve radiation bandwidth and radiation efficiency in response, slots need to be etched from the unit cell. The geometry of slots is acquired in such a manner that more than one radiating edges could be provided within the unit cell [25]. Such radiation edges will provide extra room to the electromagnetic fields to radiate in free space.

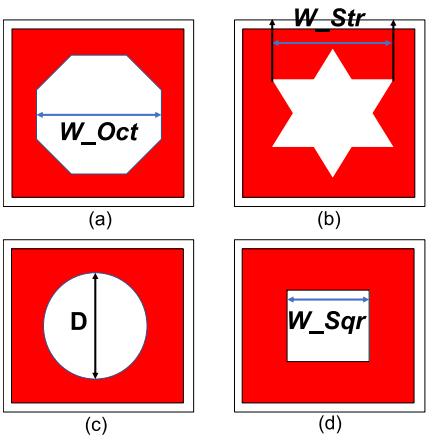

FIGURE 3. Slotted unit cells. (a) Octagon-slot unit cell, (b) Star-slot unit cell, (c) Circle-slot unit cell, (d) Square-slot unit cell.

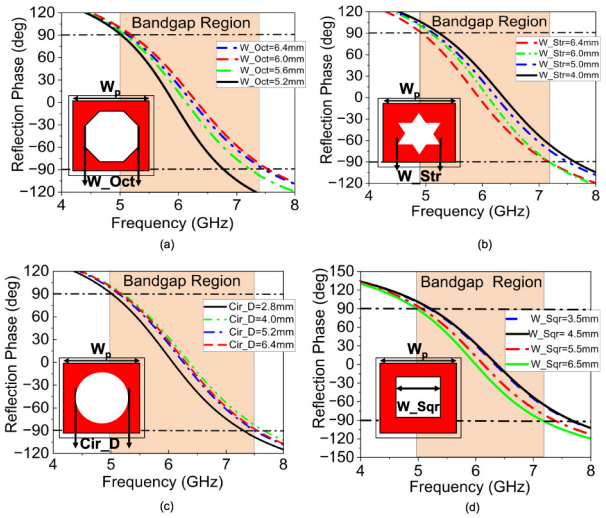

FIGURE 4. Reflection phase response of unit cells. (a) Octagon-slotted unit cell. (b) Star-slotted unit cell. (c) Circle slotted unit cell. (d) Square slotted unit cell. (W_p = 9mm).

For this purpose, different shapes such as octagon, square, circular and star shaped slot (consisting of two inverted equilateral triangles) are loaded on the unit cells in such a manner that more than one radiating edge corresponding to different frequencies in band of interest be provided within the unit cells. The dimensions of these slots relate to EHL $= \lambda_0/6.7$ for $\lambda_0 = 7$ GHz. Considering this EHL, the initial dimension of W_{Oct}, W_{Str}, D, and W_{Sqr} are taken as 6.4 mm. Each slotting geometry and dimensions are shown in Fig. 3. These dimensions are optimized afterwards and are given in Fig. 1. Again, the floquet-port analysis with same set-up is made on the slotted unit cells where the outer dimension Wp is fixed, and only the shape and size of the inner slots are changed for inspecting their effect. It can be seen in Fig. 4 that the addition of slots increases bandwidth. This wider bandgap region improves the radiation efficiency, that leads to the improvement in antenna's gain. The unit cells with the non-uniform slots are assembled to form the proposed

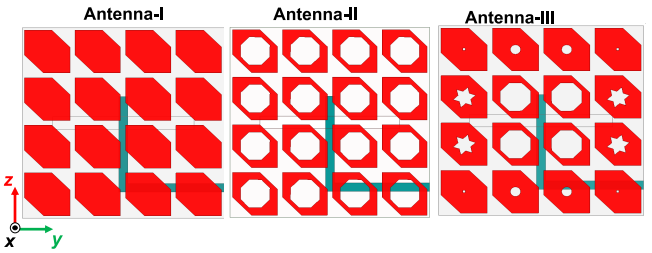

FIGURE 5. Configuration of different MTS antennas. zx is E-plane and zy is H-plane symmetry.

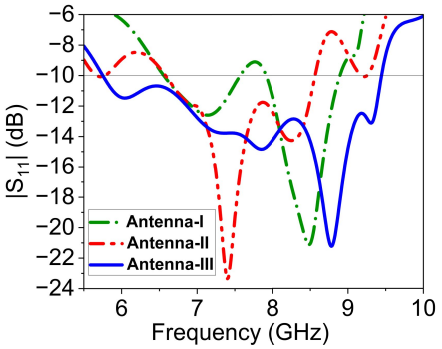

FIGURE 6. S-parameter comparison of three MTS antennas.

4 x 4 metasurface structure, as shown in Fig. 1. The specific arrangement of the slot resulting in the proposed antenna is intentional and the reason of this arrangement will be explained in Section III-B.

B. WORKING PRINCIPLE: EFFECT OF SLOTS ON MODE COUPLING

As discussed in Section III-A, the loading of non-uniform slots results in widen bandgap regions. This is attributed to the fact that these slots provide additional radiation edges corresponding to their operating frequency thereby resulting in better performance. In this regard, a performance comparison is made among three different MTS antenna configurations as shown in Fig. 5. The first structure, Antenna-I is composed of conventional 4 x 4 unit cells metasurface with truncated corners, a slotted ground plane, and a feedline. The corners of each unit cell are truncated to achieve circular polarization as will be explained in Section III-C. Antenna-II is the square-patch MTS having uniform slots while Antenna-III is the proposed MTS with slots of different geometric shapes, and sizes along with truncated corners. All three antennas have the same overall size and substrate heights. Moreover, for the fair comparison the feed location is fixed in all the cases. The $|S_{11}|$ curves of all three antennas are depicted in Fig. 6, in which, Antenna-III confirms that the proposed metasurface provides wide -10dB impedance bandwidth from 5.74 GHz to 9.44 GHz due to its nonuniform geometry.

The characteristic mode analysis (CMA) of all three antennas is performed to fully comprehend the impact of the

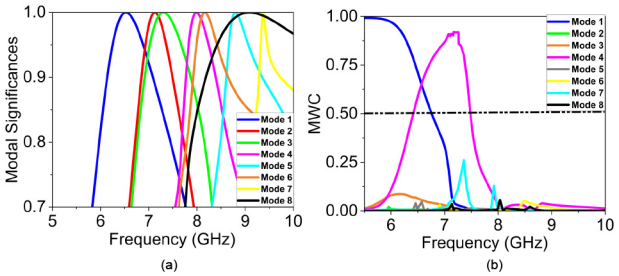

FIGURE 7. CMA of Antenna-I. (a) Modal Significances (MS). (b) Modal Weighting Coefficients (MWC).

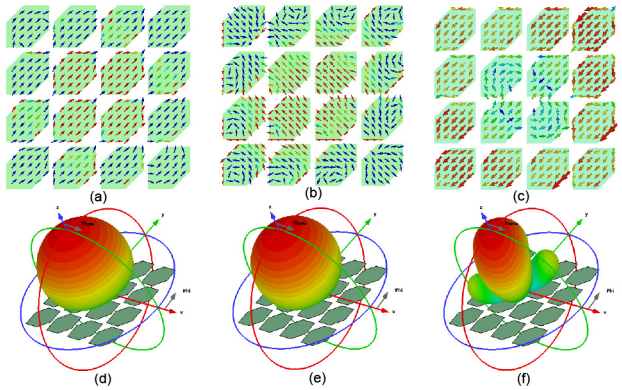

FIGURE 8. Modal current patterns of (a) Mode 1, (b) Mode 2, and (c) Mode 8. Radiation patterns of (d) Mode 1, (e) Mode 2, and (f) Mode 8.

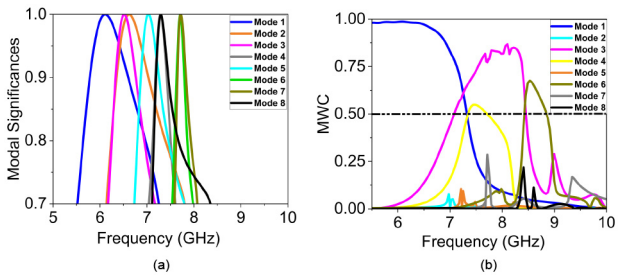

FIGURE 9. CMA of Antenna-II. (a) Modal Significances. (b) Modal Weighting Coefficients.

suggested slotting geometry over the resonance of nearby modes. More importantly, the modal current patterns of respective modes will help in adjusting the place of slots in the unit cells. To assert the claim, two important parameters, i.e., Modal Significance (MS) and Modal Weighting Coefficient (MWC) are obtained by the CMA. A mode is said to radiate if its $MS \geq 0.707$, while MWC tells how efficiently a mode is coupled to a source. A high modal weighting coefficient value over a frequency band of interest means that power is being strongly coupled to the mode. Therefore, a mode will not radiate with MS value of even 1, if its MWC value is low [18], [19]. The modal analysis is categorized into three parts respective to the antenna type. Firstly, CMA of *Antenna-I* is performed to get MS values of first eight modes, as shown in Fig. 7(a). As the aperture-coupled feeding slot (typically for magnetic coupling) is placed on the ground plane, underneath the center of MTS (shown in Fig. 1). In lieu of this concept, the analysis on the design needs to be started by undertaking the CMA in CST with feedline. In this regard, the MWC values are calculated by placing an equivalent feeding stripline surrogate along the parallel of MTS at the center, to emulate aperture-coupled feeding slot [26]. Fig. 7(b) shows the MWC values of each mode for Antenna-I. From Fig. 7(b), it can be observed that just two modes are coupled well to the source and thus can be excited properly. The rest of the modes have low MWC values. Mode 1 resonates at 6.5 GHz and has bandwidth ranging from 5.8 to 7.8 GHz (the bandwidth is determined according to the criteria that $MS \geq 0.707$). Mode 8 resonates around 8.9 GHz and has bandwidth ranging from 7.7 to nearly 11.8 GHz. The excitation of mode 8 alongwith fundamental modes (mode 1 and mode 2) is important because it exhibit broadband modal significance. Moreover, the resonances of other modes fall within the resonance domain ($MS \geq 0.707$) of mode 1 and mode 8. Therefore, we digress on the efforts needed to work on the improvement of MWC of other modes and curtail our focus on mode 1, mode 2, and mode 8. Thus, the modal current patterns and radiation pattern of mode 1, 2, and 8 are shown in Fig. 8.

The conventional technique, as reported in many articles, is the cutting of uniform slots from MTS unit cells. This improves the impedance bandwidth but up to some extent. As in case of *Antenna-II* uniform octagon slots, corresponding to EHL = $\lambda_0/6.8$ ($\lambda_0 = 7.4$ GHz), are loaded. The effect of such slotted unit cells-based MTS is evaluated in terms of MS and MWC values which is shown in Fig. 9. It can be observed that MWC values of two more modes are improved as compared with CMA of Antenna-I. This improvement incorporated 7.4GHz in the bandwidth, as verified by $|S_{11}|$ in Fig. 6. Although the bandwidth is improved, but it is not desirable as the MWC of mode 8 is still low due to mismatch between the slot dimension and mode's resonance frequency. Thus, resulting a narrowband antenna. A convenient method to increase MWC value of mode 8 requires the surface modification of MTS by loading the appropriate slots, that will enhance the bandwidth resultantly.

In *Antenna-III*, the improvement in MWC values is achieved by cutting the slots of different shapes and dimensions from the unit cells, respective to the resonant frequency of mode 8. The modal current patterns observed in Fig. 8 (c) guide to build the theoretical foundation of slotting geometries as proposed in Fig. 1. Fig. 8(c) reveals that the modal current patterns of mode 8 are stronger at the marginal patches. Hence, for improving the MWC of mode 8, the appropriate radiating edges in accordance with the mode's resonance band (where $MS \geq 0.707$) should be provided at the marginal patches. For this purpose, star, circular and square-shaped slots are cut from the marginal patches of MTS. Here, the optimized EHL value of $\lambda_0/8$ for star, circular, and square shaped slots are cut from the unit cells corresponding to λ_0 at f_o=8 GHz, f_o=8.8 GHz,

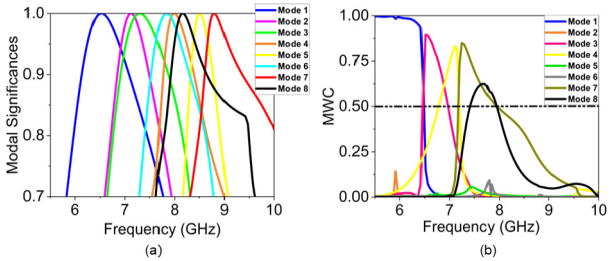

FIGURE 10. CMA of Antenna-III. (a) Modal Significances. (b) Modal Weighting Coefficients.

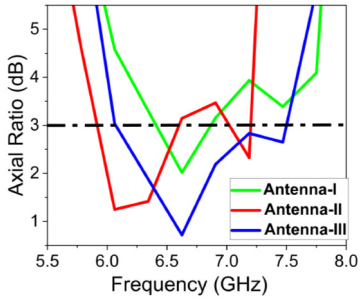

FIGURE 11. Axial ratio plots of three antennas.

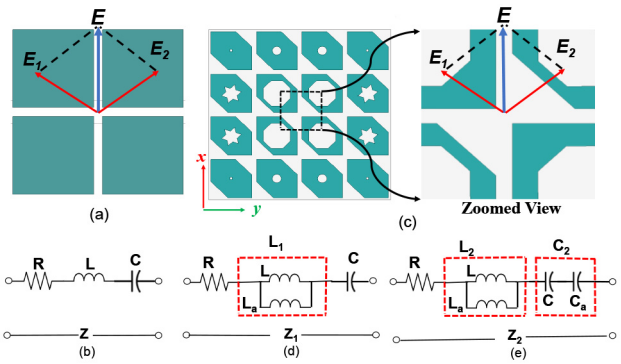

FIGURE 12. Geometric configuration and equivalent circuit models of MTS. (a), (b) Conventional MTS and it's equivalent circuit. (c) Proposed MTS and its zoomed view. (d) and (e) Equivalent circuits for impedances Z_1 and Z_2, seen by $\vec{E}_1$ and $\vec{E}_2$, respectively.

f_o=9.2 GHz, respectively. This makes W_{Str} = 3.9mm, D_{Cir} = 1.7mm, and W_{Sqr} = 0.5mm, respectively. Fig. 1 shows the MTS structure corroborating the unit cells having optimized slot dimensions respective to their frequencies. The CMA response shown in Fig. 10 demonstrates that the non-uniform slots resulted in improved mode coupling with source, thereby improving the MWC value of mode 8. Thus, non-uniform slots help to excite the resonant modes within the MTS in much effective way as compared with a uniform slot or no slot case. It should be noted here that this specific arrangement is arrived at after extensive simulations (not shown here for brevity) by studying modal currents of the modes. Also, the shape of slots within the unit cells can be selected according to the choice but their sizes should be strictly in accordance with the EHL value of each respective frequency, to get desired wide bandwidth. To summarise the design analysis, slots with larger dimensions (octagon) are loaded in the center to improve the 3-dB axial ratio bandwidth for orthogonal modes 1 and 2, while slots with other dimensions (star, square, circle) are added in the periphery to help improve the coupling of mode 8. By the help of L-shaped microstrip feedline, the proposed MTS is radiated through an aperture coupled slot in the ground plane. The L-shaped feedline structure is adopted to design a modified feed structure of array configuration based on the proposed design that will be discussed in Section VI.

C. CIRCULAR POLARIZATION

Apart from producing wider bandwidth, the non-uniform metasurface antenna also results in wider 3dB axial ratio bandwidth as compared with Antenna-I and Antenna-II shown in Fig. 11.

To shed insight into this, the phenomenon of converting a linearly polarized (LP) radiating wave from the ground slot into a circularly polarized (CP) wave through designed MTS is analyzed in this section. Due to the truncation of unit cells in the designed MTS, the LP electric field wave after passing through the MTS, is resolved into two components, i.e., $\vec{E}_1$ and $\vec{E}_2$, which are orthogonal to each other. In case of a symmetric square-patch MTS as shown in Fig. 12 (a), the impedances of both $\vec{E}_1$ and $\vec{E}_2$ will be same, i.e., Z_1=Z_2=Z where degeneracy is inculcated between mode 1 and mode 2. The equivalent circuit model for such a symmetric square-patch MTS is given in Fig. 12 (b). Incorporating the MTS with non-uniform slots and truncating the corners of the unit cells diagonally as shown in Fig. 12(c), different impedances will be produced by $\vec{E}_1$ and $\vec{E}_2$ which are given as [12]:

$$Z_1 = R_1 + jwL_1 + 1/jwC_1 \quad (1)$$

$$Z_2 = R_2 + jwL_2 + 1/jwC_2 \quad (2)$$

where C is capacitance formed by E-fields across the gap between the unit cells, L is the inductance formed by the current flowing on the patches, R is the resistance of the unit cells [12]. The equivalent circuit models for Z_1 and Z_2 are given in Fig. 12 (d) and (e), respectively. The impedance Z_1 is associated with the slot-loaded MTS unit cells without truncated corners. For this case, the imaginary part X_1 becomes less inductive. This is because the removal of conductor area from unit cells decreases inductance from L to L_1. While, for the case of slot-loaded unit cells along with truncated corners, capacitance C_2 reduced. Consequently, X_2 will become larger than X_1 according to the relations (5) and (6). Since, the reactance of Z_2 is greater than Z_1, E_2 will lead $\vec{E}_1$ by $\vec{E}_2$ - $\vec{E}_1$. The proposed MTS is designed such that $|Z_1|$=$|Z_2|$ and $\angle Z_2 - \angle Z_1 = 90^o$, so the resultant electric fields are circularly polarized. Linking this analysis with 3-dB axial ratio comparison, the results shown in Fig. 12 reveals that for Antenna-I, the difference between X_2 and X_1 is less compared to that with Antenna-III. Hence, Z_2 is not so greater than Z_1 providing $\angle Z_2 - \angle Z_1 \neq 90^o$. The 3-dB

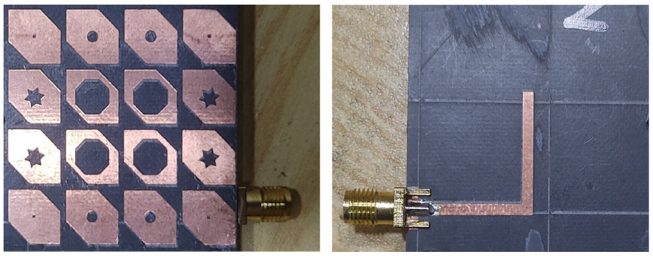

FIGURE 13. Fabricated prototype of the proposed non-uniform MTS-based antenna.

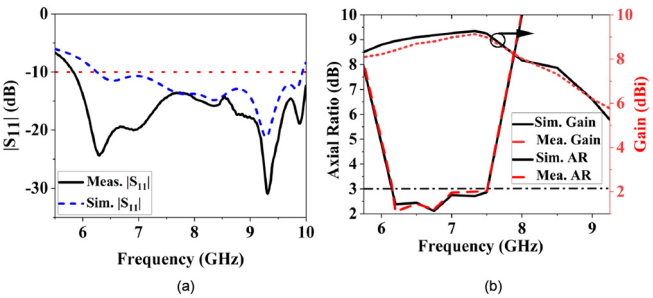

FIGURE 14. Simulated and Measured results of the proposed MTS antenna. (a) S-parameters. (b) Gain and Axial ratio.

axial ratio results of Antenna-II did not improve due to the narrowness of resonance bands, as shown in Fig. 9 (a).

IV. EXPERIMENTAL RESULTS AND DISCUSSIONS

The proposed non-uniform metasurface-based antenna is designed, fabricated, and measured. The fabricated prototype is shown in Fig. 13. The measured and simulated results of the prototype are depicted in Fig. 14. As shown in Fig. 14 (a), the measured impedance bandwidth for $|S_{11}| \leq -10$ is 48.74%. Fig. 14 (b) reveals that the measured 3 dB axial ratio bandwidth is 19.92%. And the measured peak gain of 9.35 dBi is observed at 7.33 GHz. Fig. 15. (a) and (b) show the measured and simulated radiation patterns for both E- and H-planes at 6 GHz and 7.33 GHz, respectively. The results reveal that the antenna produces symmetric and stable broadside radiation patterns.

V. ARRAY DESIGN AND RESULTS

Based on the proposed metasurface antenna element, a 2 x 2 antenna array is designed and analyzed experimentally to achieve further high gain and wide axial ratio bandwidth. A modified sequential phase feed (SPF) network based on L-shaped feed is designed and used to excite 2 x 2 array elements. The SPF network act as a quarter wavelength transformer, which was specifically designed to achieve impedance matching between input and outputs by distributing the signal from input (microstrip-line) to four outputs having the phases of 0°, 90°, 180°, 270° [21]. In the design procedure, four elements of the proposed metasurface are placed in a sequentially rotated arrangement, so that they can be properly incorporated into the SPF network to achieve

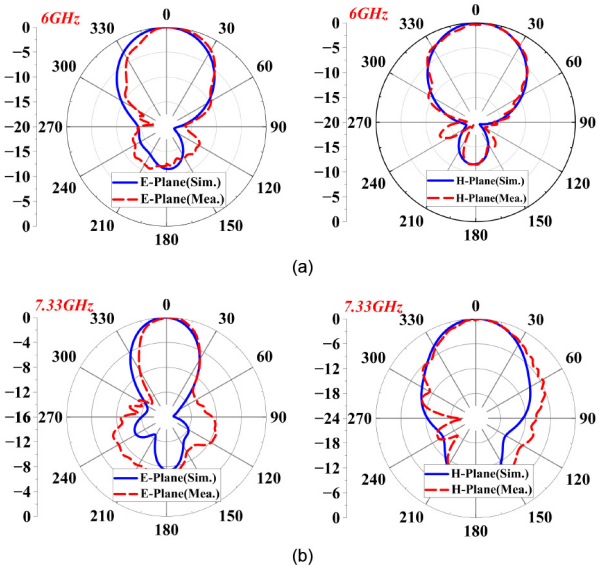

FIGURE 15. Simulated and measured radiation patterns of the proposed MTS-antenna in E-/H-Planes at (a) 6 GHz and (b) 7.33 GHz.

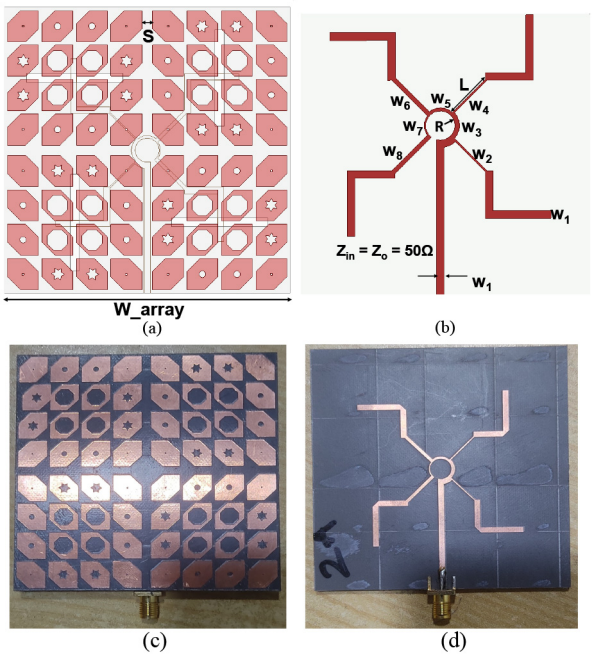

FIGURE 16. Configuration of 2 x 2 array model. (a) Front-view. (b) Back-view. (c) Front-view of a fabricated model. (d) Back-view of a fabricated model. (W_{array} = 83mm, S = 3mm, R = 3.5mm, wf = w1= 1.81mm, w2 = w4= 0.4mm, w3 = 1.1mm, w5 = 0.74mm, w6=w8= 1mm, w7= 0.376mm, L=11.7mm).

the required wide axial ratio bandwidth performance. The optimized center-to-center space 'S' of 3mm was selected to achieve improved radiation patterns with low side lob levels. The designed array and its fabricated prototype are shown in Fig. 16.

Fig. 17 shows the measured and simulated results of impedance bandwidth, 3 dB axial ratio bandwidth, and gain of the array configuration. The results reveal that for the impedance bandwidth of 4.50-9.58 GHz (71.74%), the array

TABLE 1. Performance comparison of single element MTS-based antennas.

Ref.	Size (λ_o^3)	Freq. (GHz)	$\|S_{11}\|\leq$-10 BW (%)	AR BW (%)	Peak Gain (dBi)	RE (%)
[4]	0.8x0.8x0.06	5.8	4.7-7.2 (42.1%)	5.1-6.9 (30%)	7.6	-
[5]	0.58x0.58x0.056	5.5	4.7-7.48 (45.6%)	4.9-6.2 (23.4%)	7.6	90
[6]	0.48x0.48x0.057	5.9	4.05-6.6 (43.22%)	5.3-6.6 (22%)	6.16	70
[7]	0.71x0.71x0.038	5.1	3.75-6.67 (55.7%)	4.38-5.98 (31.37%)	7	93
[10]	1.4x1.4x0.072	5.6	4.5-5.8 (38.8%)	5.2-6 (14.3%)	8.5	90
[11]	0.65x0.65x0.06	5.5	4.28-6.37 (39.25%)	5.18-6.19 (17.77%)	6.8	88
[15]	1x1x0.058	5.5	4.86-6.26 (25.08%)	5.30-6.43 19.4%	8	-
[24]	0.67x0.67x0.068	2	1.98-2.37 (17.44%)	1.99-2.37 (17.43%)	8	96
Proposed Single Element	**0.8x0.8x0.079**	**6**	**5.74-9.44 (48.84%)**	**6.19-7.56 (19.92%)**	**9.35**	**96.6**
Performance Comparison of 2x2 MTS Array Antennas						
[20]	1.26x1.26x0.046	5.9	4.4-8.00 (55.6%)	4.8-7.0 (41.67%)	12.08	88
[21]	1.22x1.22x0.15	4.8	3.6-6.2 (53.1%)	3.7-4.8 (28.32%)	6.3	88
[22]	1.53x1.53x0.08	5.9	4-8.4 (74.57%)	4.3-7.63 (56.4%)	10.04	60
[23]	1.6x1.6x0.065	9.6	7.88–12 (41.45%)	8.6-10.8 (22.68%)	13.50	>84
Proposed Array	**1.38x1.38x0.066**	**5**	**4.50-9.58 (71.74%)**	**4.50-8.52 (61.75%)**	**14.45**	**96.9**

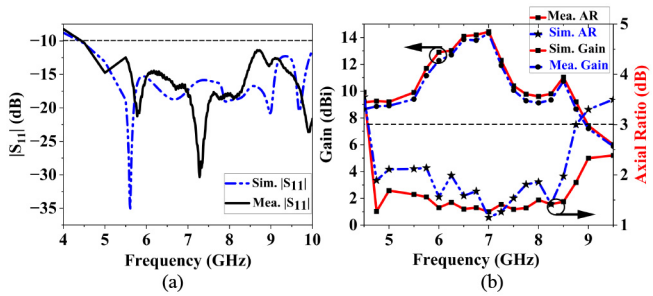

FIGURE 17. Simulated and measured results of the antenna array. (a) S-parameters. (b) Gain and axial ratio.

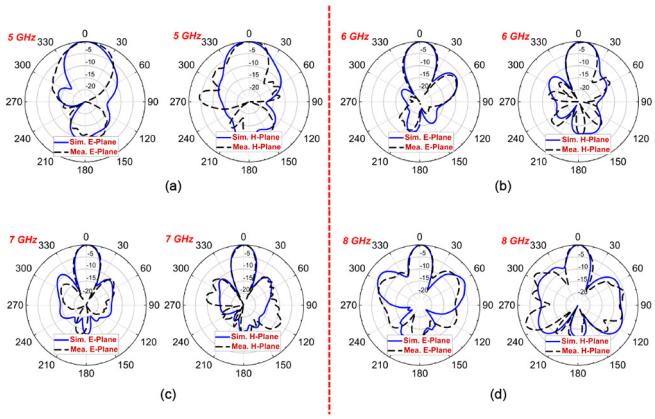

FIGURE 18. Simulated and measured radiation patterns of the proposed MTS-array antenna in E-/H-Planes at (a) 5 GHz, (b) 6 GHz, (c) 7 GHz, (d) 8 GHz.

produced wide AR bandwidth of 61.75% (4.50-8.52 GHz) with a peak gain of 14.45 dBi. Fig. 18. depicts both simulated and measured radiation patterns at different frequencies of 5 GHz, 6 GHz, 7 GHz, and 8 GHz. The designed array produced stable radiation patterns with circularly polarized radiations. Table 1 provides a detailed comparison of the proposed antenna with other MTS-based antenna designs. The comparison reveals that the proposed antenna is circular polarized, compact, low profile, with wide bandwidth, and high gain over the CP band.

VI. CONCLUSION

In this work, an MTS-based low-profile, wideband, high gain, and circularly polarized antenna is presented. The wide bandwidth is obtained through improved mode coupling using nonuniform slots. Thus, for fixed feed location surface modification through slots provides extra degree of freedom to obtain wider bandwidth. The antenna is verified through fabrication and measured results show good agreement with the simulated ones. Furthermore, a 2 x 2 MTS-array is designed and validated resulting in higher peak gain and wider 3 dB axial ratio bandwidth. The improved performance matrices of the proposed antenna and it array configuration distinguish them from similar antennas reported in the literature. These antennas find good use in modern wireless communication systems, such as WiMAX, long-range tracking, and C-band applications.

REFERENCES

[1] C.-L. Mak, H. Wong, and K.-L. Luk, "High-gain and wideband single layer patch antenna for wireless communications," *IEEE Trans. Veh. Technol.*, vol. 54, no. 1, pp. 33–40, Jan. 2005.

[2] E. Nishiyama and M. Aikawa, "Wide-band and high-gain microstrip antenna with thick parasitic patch substrate," in *Proc. IEEE Antennas Propag. Soc. Int. Symp.*, 2004, pp. 273–276.

[3] K. M. Luk, C. L. Mak, Y. L. Chow, and K. F. Lee, "Broadband microstrip patch antenna," *Electron. Lett.*, vol. 34, no. 15, pp. 1442–1443, Jul. 1998.

[4] S. X. Ta and I. Park, "Low-profile broadband circularly polarized patch antenna using metasurface," *IEEE Trans. Antennas Propag.*, vol. 63, no. 12, pp. 5929–5934, Dec. 2015, doi: 10.1109/TAP.2015.2487993.

[5] T. T. Le, H. H. Tran, and A. A. Althuwayb, "Wideband circularly polarized antenna based on a non-uniform metasurface," *Appl. Sci.*, vol. 10, no. 23, p. 8652, 2020. [Online]. Available: https://doi.org/10.3390/app10238652

[6] N. Supreeyatitikul, T. Lertwiriyaprapa, and C. Phongcharoenpanich, "S-shaped metasurface-based wideband circularly polarized patch antenna for C-band applications," *IEEE Access*, vol. 9, pp. 23944–23955, 2021, doi: 10.1109/ACCESS.2021.3056485.

[7] C. H. S. Nkimbeng, H. Wang, and I. Park, "Low-profile wideband unidirectional circularly polarized metasurface-based bowtie slot antenna," *IEEE Access*, vol. 9, pp. 134743–134752, 2021, doi: 10.1109/ACCESS.2021.3116714.

[8] W. Cao, X. Lv, Q. Wang, Y. Zhao, and X. Yang, "Wideband circularly polarized Fabry–Perot resonator antenna in Ku-band," *IEEE Antennas Wireless Propag. Lett.*, vol. 18, no. 4, pp. 586–590, Apr. 2019.

[9] P. Xie, G. Wang, X. Zou, and B. Zong, "Gain and AR improvements of the wideband circularly polarized Fabry–Perot resonator antenna," *IEEE Trans. Antennas Propag.*, vol. 69, no. 10, pp. 6965–6970, Oct. 2021, doi: 10.1109/TAP.2021.3076573.

[10] C. Zhao and C.-F. Wang, "Characteristic mode design of wide band circularly polarized patch antenna consisting of H-shaped unit cells," *IEEE Access*, vol. 6, pp. 25292–25299, 2018, doi: 10.1109/ACCESS.2018.2828878.

[11] J. Dong, C. Ding, and J. Mo, "A low-profile wideband linear-to-circular polarization conversion slot antenna using metasurface" *Materials*, vol. 13, no. 5, p. 1164, 2020. [Online]. Available: https://doi.org/10.3390/ma13051164

[12] C. Ni, M. S. Chen, Z. X. Zhang, and X. L. Wu, "Design of frequency- and polarization-reconfigurable antenna based on the polarization conversion metasurface," *IEEE Antennas Wireless Propag. Lett.*, vol. 17, pp. 78–81, 2018, doi: 10.1109/LAWP.2017.2775444.

[13] F. H. Lin and Z. N. Chen, "Low-profile wideband metasurface antennas using characteristic mode analysis," *IEEE Trans. Antennas Propag.*, vol. 65, no. 4, pp. 1706–1713, Apr. 2017, doi: 10.1109/TAP.2017.2671036.
[14] D. Chen, W. Yang, W. Che, and Q. Xue, "Broadband stable-gain multiresonance antenna using nonperiodic square-ring metasurface," *IEEE Antennas Wireless Propag. Lett.*, vol. 18, pp. 1537–1541, 2019, doi: 10.1109/LAWP.2019.2919692.
[15] A. E. Yousfi, A. Lamkaddem, K. A. Abdalmalak, and D. Segovia-Vargas, "A broadband circularly-polarized single-layer metasurface antenna using characteristic mode analysis," *IEEE Trans. Antennas Propag.*, vol. 71, no. 4, pp. 3114–3122, Apr. 2023, doi: 10.1109/TAP.2023.3239104.
[16] D. Sievenpiper, L. Zhang, R. F. J. Broas, N. G. Alexopolous, and E. Yablonovitch, "High-impedance electromagnetic surfaces with a forbidden frequency band," *IEEE Trans. Microw. Theory Techn.*, vol. 47, no. 11, pp. 2059–2074, Nov. 1999, doi: 10.1109/22.798001.
[17] M. Vogel, G. Gampala, D. Ludick, U. Jakobus, and C. J. Reddy, "Characteristic mode analysis: Putting physics back into simulation," *IEEE Antennas Propag. Mag.*, vol. 57, no. 2, pp. 307–317, Apr. 2015, doi: 10.1109/MAP.2015.2414670.
[18] D. Fazal and Q. U. Khan, "Dual-band dual-polarized patch antenna using characteristic mode analysis," *IEEE Trans. Antennas Propag.*, vol. 70, no. 3, pp. 2271–2276, Mar. 2022, doi: 10.1109/TAP.2021.3111341.
[19] Y. Chen and C.-F. Wang, *Charasteristic Modes: Theory and Applications in Antenna Engineering*. Hoboken, NJ, USA: Wiley-IEEE, 2015.
[20] S. X. Ta and I. Park, "Compact wideband circularly polarized patch antenna array using metasurface," *IEEE Antennas Wireless Propag. Lett.*, vol. 16, pp. 1932–1936, 2017, doi: 10.1109/LAWP.2017.2689161.
[21] S. Wang, H. Hao, X. Ma, H. Cheng, and X. Huang, "Wideband circularly polarized array antenna based on sequential phase feeding metasurfaces for 5G (sub-6G) applications," *J. Electromagnet. Waves Appl.*, vol. 37, no. 1, pp. 15–24, 2022, doi: 10.1080/09205071.2022.2110948.
[22] N. Supreeyatitikul, D. Torrungrueng, and C. Phongcharoenpanich, "Quadri-cluster broadband circularly-polarized sequentially-rotated metasurface-based antenna array for C-band satellite communications," *IEEE Access*, vol. 9, pp. 67015–67027, 2021, doi: 10.1109/ACCESS.2021.3075994.
[23] S. X. Ta and I. Park, "Planar wideband circularly polarized metasurface-based antenna array," *J. Electromagnet. Waves Appl.*, vol. 30, no. 12, pp. 1620–1630, 2016. [Online]. Available: https://doi.org/10.1080/09205071.2016.1210038
[24] F. A. Dicandia and S. Genovesi, "Characteristic modes analysis of non-uniform metasurface superstrate for nanosatellite antenna design," *IEEE Access*, vol. 8, pp. 176050–176061, 2020, doi: 10.1109/ACCESS.2020.3027251.
[25] Q. U. Khan, D. Fazal, and M. Bin Ihsan, "Use of slots to improve performance of patch in terms of gain and Sidelobes reduction," *IEEE Antennas Wireless Propag. Lett.*, vol. 14, pp. 422–425, 2015, doi: 10.1109/LAWP.2014.2365588.
[26] H. Alroughani and D. A. McNamara, "The shape synthesis of dielectric resonator antennas," *IEEE Trans. Antennas Propag.*, vol. 68, no. 8, pp. 5766–5777, Aug. 2020, doi: 10.1109/TAP.2020.2988984.

KOMAL IQBAL received the B.S. degree in electronics engineering from the University of Engineering and Technology, Taxila, Pakistan, in 2018, and the master's degree in electrical engineering from the College of Electrical and Mechanical Engineering, CEME, NUST, Pakistan, in 2023. She is currently pursuing the Ph.D. degree in terahertz communications, electrical engineering with the University of Adelaide, SA, Australia. Her research interest includes wireless communication, metasurface-based antenna designing, terahertz antennas, and communication frontends in terahertz. She was a recipient "Scotland Pakistan Scholarships for Young Women and Girls, Master's/M.phil."

QASIM UMAR KHAN (Member, IEEE) received the B.E. and M.S. degrees in computer systems and electrical engineering from the College of EME, National University of Sciences and Technology (NUST), Pakistan, in 2009 and 2011, respectively, and the Ph.D. degree in electrical engineering from NUST, where he is currently serving as an Associate Professor. He has worked on antenna projects, including MIMO antenna design for millimeter wave applications shared aperture antenna for sub 6 GHz and millimeter wave applications. He is currently working on high gain wideband circularly polarized metasurface-based antenna and a low-cost wide-angle beam scanning SIW leaky wave metasurface based antenna. He has published over 50 articles in many reputed journals and conference. His research interests include digital communication and digital signal processing, planar antenna designs, microwave devices, metasurfaces-based antennas, and leaky wave antennas. He was awarded with best teacher and best community service awards. He was also recipient of the undergraduate scholarship of his university.

ZUBAIR AHMED received the B.Sc. and M.Sc. degrees in electrical engineering from the National University of Sciences and Technology (NUST), Pakistan, in 2003 and 2008, respectively, and the Ph.D. degree in electrical engineering from the Capital University of Science and Technology, Pakistan, in 2021. He joined the Department of Electrical Engineering, College of Electrical and Mechanical Engineering, NUST in 2010. He is a Senior Member of Microwave Engineering Research Laboratory. His current research interest includes high gain patch antennas, transmit and reflectarray antennas, multibeam antennas, filtering antennas, and integrated RF front ends.